Lab on a Chip

Cite this: *Lab Chip*, 2011, **11**, 4214

www.rsc.org/loc

PAPER

Multiplexing superparamagnetic beads driven by multi-frequency ratchets†

Lu Gao,[a] Mukarram A. Tahir,[a] Lawrence N. Virgin[a] and Benjamin B. Yellen[ab]

Received 25th July 2011, Accepted 4th October 2011
DOI: 10.1039/c1lc20683d

Here, we explore the single particle dynamics of superparamagnetic beads exposed to multifrequency ratchets. Through a combination of theory, simulation, and experiment, we determine the important tuning parameters that can be used to implement multiplexed separation of polydisperse colloidal mixtures. In particular, our results demonstrate that the ratio of driving frequencies controls the transition between open and closed trajectories that allow particles to be transported across a substrate. We also demonstrate that the phase difference between the two frequencies controls not only the direction of motion but also which particles are allowed to move within a polydisperse mixture. These results represent a fundamentally different approach to colloidal separation than the previous methods which are based on controlling transitions between phase-locked and phase-slipping regimes, and have a higher degree of multiplexing capabilities that can benefit the fields of biological separation and sensing as well as provide crucial insights into general ratchet behavior.

I. Introduction

Transporting and multiplexing the motion of small objects in a micro-chip platform, including colloidal particles, cells and bacteria, can enhance the flexibility of lab-on-a-chip devices, allowing for new functions such as micro-scale flow cytometry, and improved mechanisms for sorting rare biological materials from polydisperse mixtures. Magnetic flow based sorting systems have demonstrated feasibility of sorting multiple magnetic objects by controlling the residence time in a flow stream,[1–4] but these systems suffer from several technical problems, including: (i) the highly nonlinear position-dependent nature of magnetic forces, which complicates efforts to move the magnetically labeled cells or particles across the flow stream at a uniform and reproducible rate; and (ii) magnetic flow based cell sorting is extremely sensitive to external parameters including the background matrix (*e.g.* changes in viscosity, flow speed,[5] *etc.*) as well as variations in cellular parameters (particle loading rate, cell size, *etc.*).

The use of synchronization phenomena and ratchet behavior overcomes these challenges by promoting the suspended particles or cells to move at a highly reproducible speed across the substrate, irrespective of the external medium, when sufficiently low operating frequencies are applied. Past work on ratchet systems have primarily used electric,[6,7] magnetic,[8–16] and optical[17–22] fields for controlling colloidal particles; however some of the most promising candidates are ratchet substrates that retain "memory" without external power, including magnetic[8–15] and ferroelectric micro-patterns, which allow implementation of diverse functions on a massively parallel scale without the requirement of electrical wiring patterns or the interference of multiple optical beams, which increase cost and complexity and reduce available chip space. An additional motivation for magnetic manipulation of colloids is the ability to use quasi-static (low frequency) fields that do not heat the fluid or introduce electrochemical flows.[4]

Ratchet phenomena is a broad topic that uses time modulated periodic potential energy landscapes to control the motion of various mobile components (particles), ranging from electrons,[23] spins,[24–27] atoms,[28–30] as well as molecules, colloidal particles[6,10,12–16,18,31,32] and biological materials.[6,12,15,16,33] Time modulation of the landscape is typically accomplished with an external electric, optical, magnetic, acoustic, thermal, or fluidic source field and used to rectify one type of motion (*e.g.*, external field rotation) into another type (*e.g.*, particle translation).[12] A rich display of synchronization has been observed in these systems as a result of the periodicities of the underlying landscape and the various modes of excitation (monochromatic, multichromatic, white noise, *etc.*). Rectified particle flux in spatially asymmetric landscapes has been observed in systems such as colloidal and molecular motion inside asymmetric pores[32,33] and above asymmetric electric potentials,[34,35] electron and atom motion in quantum ratchets,[23,28,36] spin transport in superconductors,[27] and many others.

To date, a major challenge in the development of high efficiency ratchet based magnetic sorting systems is to develop techniques that can selectively activate one type among different

[a]*Department of Mechanical Engineering and Materials Science, Center for Biologically Inspired Materials and Material Systems, Duke University, Durham, North Carolina, 27708, USA*
[b]*University of Michigan-Shanghai Jiao Tong Joint Institute, Shanghai Jiao Tong University, Shanghai, 200040, People's Republic of China*
† Electronic supplementary information (ESI) available. See DOI: 10.1039/c1lc20683d

types of magnetic objects on a chip. Past exploration of magnetic ratchet based separation mechanisms have exploited the bifurcation between phase-locked and phase slipping dynamic regimes to achieve differential motion between two bead types.[10,12] When the driving frequency is held below a critical threshold, which depends on the bead size and its magnetic properties, the beads synchronize with the external fields and move across the substrate at a rate determined entirely by the driving frequency (phase-locked state). Conversely, when the driving frequency is above a critical threshold, the beads are no longer able to synchronize with the external drive and slip out of local potential energy minima (phase-slipping state) leading to reduced velocity and in some cases zero time-average velocity.[10,11] These results are certainly promising; however the separation modality is asymmetric in the sense that larger (or more magnetic) objects will remain mobile at higher frequencies, whereas smaller (or less magnetic) objects will not. The utilization of a different type of control parameter (in our case, the phase difference between multifrequency driving fields) can improve the symmetry of the separation method by allowing the smaller beads to move at the expense of the bigger beads at one phase, and *vice versa* at another phase. This new control mechanism opens up new opportunities for improving the multiplexing capabilities of magnetic sorting systems.

The work presented here was inspired by recent experimental observations,[14] which showed the possibility of using multifrequency excitation to achieve differential motion within two different particle types on a common ratchet substrate. Despite these very interesting early observations, a systematic evaluation was not conducted nor was a general theory put forward to explain this behavior or predict other possible dynamic modes. As an additional purely scientific motivation, multifrequency ratchets[25,26,29,30] have fascinating dynamic phenomena that have been observed in other physical systems, including the motion of flux quanta and the cold atoms in optical traps, but have not been studied carefully at the single particle level. Magnetic colloidal particles are a highly accessible experimental model for real-time exploration of the ratchet based particle transport properties at the single particle level due to the ease of tracking multiple particles with video microscopy. Therefore this system is not only of relevance to applications in bioseparation and sensing,[12] but also allows for the fundamental properties of various ratchet conditions to be experimentally studied.

II. Computational model

The experimental system shown in Fig. 1 consists of a rectangular lattice of identical micro-magnets (with lattice spacial period d) uniformly magnetized in the same direction. For simplicity, we treat each micro-magnet as two opposite magnetic point poles separated by the magnet diameter, d_M, with the array pole density expressed as:

$$\lambda(\xi_x,\xi_y) = \lambda_0 \sum_{m=-\infty}^{\infty}\sum_{n=1}^{\infty}[\cos(n\xi_x) - \cos(n\xi_x - n\xi_M)]\cos(m\xi_y) \tag{1}$$

where n and m are integers representing the different spatial Fourier frequencies of an array of point poles along the x and y- directions, respectively, and λ_0 is the effective magnetic pole density, which is a constant that depends on the film thickness, magnetization, and shape. For convenience, we adopt the following shorthand notation where $\vec{\xi} = 2\pi\vec{r}/d = [\xi_x,\xi_y,\xi_z]$ is the dimensionless position vector and $\xi_M = 2\pi d_M/d$ is the ratio of the magnet diameter to lattice period.

The field produced by the substrate is solved through separation of variables and matching the boundary conditions of eqn (1). To externally drive the system, we apply additional uniform magnetic field, $\vec{H}_{ext}$, consisting of two orthogonal fields H_x and H_z oscillating at frequencies ω_x and ω_z respectively. The frequency ratio, $R_f = \omega_z/\omega_x$, is applied with an initial phase difference, φ_0, allowing the total magnetic field to be expressed as:

$$\vec{H}_{tot}(\vec{\xi},t) = \begin{bmatrix} H_0\sin(\omega_x t) \\ 0 \\ H_0\sin(\omega_z t + \varphi_0) \end{bmatrix} + \begin{bmatrix} \lambda_0 \sum_{m=-\infty}^{\infty}\sum_{n=1}^{\infty}\frac{n}{N}v_n(\xi_x)\cos(m\xi_y)e^{-N\xi_z} \\ \lambda_0 \sum_{m=-\infty}^{\infty}\sum_{n=1}^{\infty}\frac{m}{N}u_n(\xi_x)\sin(m\xi_y)e^{-N\xi_z} \\ \lambda_0 \sum_{m=-\infty}^{\infty}\sum_{n=1}^{\infty}u_n(\xi_x)\cos(m\xi_y)e^{-N\xi_z} \end{bmatrix} \tag{2}$$

where the short handed expressions $N = (n^2 + m^2)^{1/2}$, $u_n(\xi_x) = \cos(n\xi_x) - \cos(n\xi_x - n\xi_M)$, and $v_n(\xi_x) = \sin(n\xi_x) - \sin(n\xi_x - n\xi_M)$ are used for notational convenience.[11]

The magnetic force on the bead is modeled as a point dipole $\vec{m}$ in a magnetic field gradient, $\vec{F} = \mu_0(\vec{m}\cdot\nabla)\vec{H}_{tot}$, which is reasonable for a spherical bead exposed to weakly inhomogeneous magnetic fields. The dipole moment of the bead is given by $\vec{m} = 3V_p\bar{\chi}\vec{H}$, where V_p denotes the particle volume and $\bar{\chi} = 3\chi/(\chi + 3)$ denotes the shape-corrected magnetic bead susceptibility.[37] Since any restoring force will return the bead to the y-axis, we assume $y = 0$ in all simulations. Due to imperfections within the magnetization of individual micro-magnets, there is some motion in the y-direction in the experimental studies shown in Section IV; however this motion is small compared with the dimensions of the array period, and from a computational standpoint the omission of forces in the y-direction allow for more analytically tractable solutions to be obtained, which are shown to agree well with experiments. Additionally, we assume the bead is positioned exactly one bead radius above the substrate ($z = a$), since the force in the z-direction is usually negative. Thus, the force in the x-direction is expressed as:

$$F_x(\xi_x,t) = F_0\sum_{m=-\infty}^{\infty}\sum_{n=1}^{\infty}\left[\frac{n^2}{N}u_n(\xi_x)\sin(\omega_x t) - nv_n(\xi_x)\sin(\omega_z t + \varphi_0)\right]e^{-2\pi N\beta} \tag{3}$$

where $F_0 = 8\pi^2\mu_0\bar{\chi}a^3\lambda_0 H_0/3d$ and $\beta = a/d$ represent the ratio of the bead radius to the lattice period. For colloids larger than 1μm that are exposed to strong forcing, Brownian motion is negligible and viscous effects tend to dominate inertial effects. We assume fluid damping results from Stoke's drag on a sphere and the bead velocity is thereby determined from first order equations of

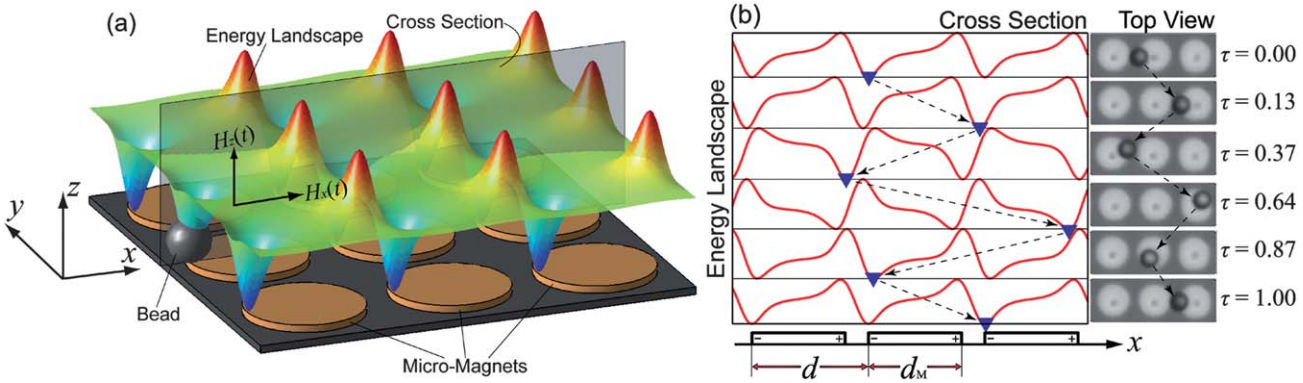

Fig. 1 System Illustration (a) Graphical depiction of the magnetostatic potential energy landscape above an array of micro-magnets. A bead (grey circle) is depicted near one pole of a micro-magnet (disks). **(b)** The potential energy landscape for the cross section specified in **(a)** is plotted at different time intervals for a frequency ratio of R_f 7/5. The red lines depict the numerically simulated potential energy landscape, and the blue ▼ symbols show the calculated position of the bead at each time point. The right hand side of **(b)** shows a series of experimental images that correspond to the bead's calculated positions. An animation of the bead's motion is provided in (SI-1).

motion, $\dot{x} = F_x/6\pi\eta a$, where η is the fluid viscosity. The bead's trajectory is computed through finite time difference implemented with a Runge–Kutta integrator. The time averaged velocity of the bead is determined through the displacement of the bead's position after a large number of cycles with respect to the oscillations of the x-field component, *i.e.*, $N_{\text{cycle}} = t \cdot f_x$.

III. Experimental methods

Substrate fabrication

To create a permanent magnetization within the array, we developed high coercivity magnetic substrates, which are less susceptible to re-magnetization in fields above 20∼30Oe than those used in our prior works. The fabricated magnetic thin film consists of a multilayer stack of 40 alternating layers of 9 Å Pt and 8 Å Co, which are shown to resist re-magnetization in external fields exceeding 100Oe.[38] The magnetic lattice was fabricated by conventional photolithographic lift-off technique using thin film deposition *via* Molecular Beam Epitaxy (MBE) at the MBE Thin Film Deposition Service Center at North Carolina State University. In all experiments, the diameter of the magnets was $d_M = 6.4\mu m$ with lattice period $d = 8.0\mu m$.

Magnetic field control

The external field apparatus used to apply the multi-frequency fields is described in our prior works.[10,12] Briefly, two 6-cm diameter solenoid coils with iron cores were arranged opposite of the chip to provide external uniform field along the x- direction. An additional identical solenoid was place below the chip to provide external uniform field along the z-direction. An image of our experimental apparatus is provided in Fig. 2. In these experiments, the external magnetic fields with magnitude $H_x = H_z = 50$Oe were applied by passing electrical current through the solenoids. The fields were measured with a handheld Gaussmeter (Lake Shore Cryotronics, Inc.) and we verified that the field variation was only a few percent across the chip. In all experiments, we applied a fixed frequency of 0.5Hz (where $\omega_{x,z} = 2\pi f_{x,z}$) to the horizontal coils, while a variable frequency was applied to the vertical coils in order to control the frequency ratio, R_f. The fields were controlled with a dual axis current controller (Cyberresearch card) and programmed with LabView®.

Multiplexed bead motion

Magnetic beads with a mean diameter of 2.7μm and magnetic susceptibility $\chi = 0.17$ (Dynabead® M-270, Invitrogen Inc.™) and beads with mean diameter of 5.8μm purchased from Bangs Laboratories™ (COMPEL™ UMC3N/9839) were used to demonstrate multiplexed phase-modulated magnetic separation. The bead suspension is confined by Secure-Seal ™ spacer (9mm in diameter and 0.12mm in depth, Invitrogen Inc.™) that was attached on the pre-patterned substrate. All the experiments are performed at room temperature and the stock beads were diluted 100 fold with de-ionized water, having a viscosity of $\eta = 0.01$ Poise.

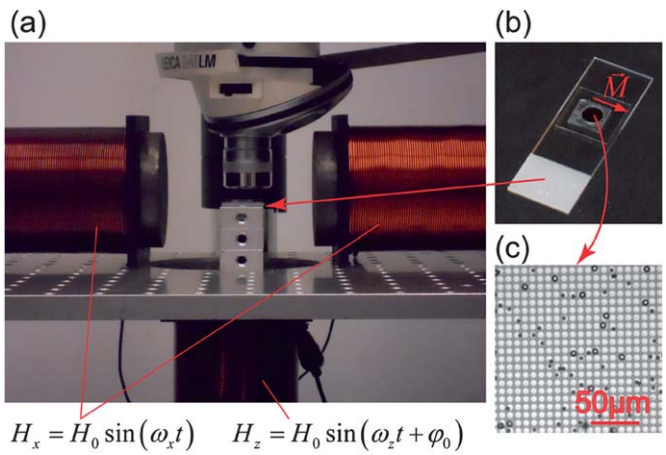

Fig. 2 Experiment Set-up. (a) The sample is placed beneath an objective and two solenoid coils are positioned on either side of the chip to provide uniform fields in the x-direction. An additional vertically oriented solenoid placed below the sample provides uniform field in the z-direction. Image **(b)** depicts the micro-array substrate on a glass slide. Image **(c)** depicts a microscopy image of a mixed suspension of 2.7-μm and 5.8-μm superparamagnetic beads resting on the micro-array.

Video tracking and trajectory analysis

A LEICA DM LM microscope (Leica MICROSYSTEMS) with 40x objective in bright field mode was used to image the experimental system. The experiments were recorded with a QIMAGING® Retiga 2000R fast camera and SimplePCI software (Hamamatsu Photonic K.K) was employed to record the trajectory of multiple beads simultaneously. Image-Pro® software (MediaCybernetics®) was used for the post-processing of the bead trajectories. We use a frame rate of 4 frames per second in order to capture the long time average of bead trajectories over a large area. This was sufficient for capturing the details of the bead's motion, which had relatively small velocities, $V_0 = F_0/6\pi\eta a \sim 10\mu m\ s^{-1}$.

IV. Results

In numerical simulations, we first analyzed the conditions that would lead to open trajectories (time-averaged net velocity of beads across the substrate) *vs.* closed trajectories (zero time-averaged bead velocity). We found that open trajectories were quite rare, only occurring at odd integer frequency ratios, which is consistent with prior work on other multifrequency ratchets.[29,30] The velocity spectra as a function of R_f is shown in Fig. 3, along with experimental data of 2.7μm diameter beads (× and ○ markers represent open and closed trajectories). The magnitude of the time averaged velocities for the different frequency ratios is given in dimensionless form by:

$$\langle V\rangle = \begin{cases} \dfrac{(-1)^P}{2P+1} & \text{for } R_f = \dfrac{2Q+1}{2P+1} \\ 0 & \text{otherwise} \end{cases} \quad (4)$$

where $P, Q = 0, 1, 2, 3\ldots$; $(2Q + 1)/(2P + 1)$ is the frequency ratio and where $2Q + 1$ and $2P + 1$ are relatively prime. Provided the driving frequency is kept sufficiently low, which allows the beads to remain phase-locked with the driving potential, the magnitude of the driving frequencies is unessential and only their ratio is important. We note here that the magnetic field must be kept above a certain threshold such that the external field induced forces are significantly larger than the static magnetic forces due to the micro-magnet array; however in past work we have observed that relatively low fields (in the range of tens of Gauss) are sufficient for this purpose.[9,10,12]

Fig. 4 provides a comparison of the experimental trajectories with the numerically simulated trajectories, and the strong agreement between theory and experiment is evident. We plot the figures using dimensionless potion $X = x / d$ in order to represent the trajectory in terms of the number of magnets traveled. Examples of open trajectories are provided in Fig. 4 [A∼H] for typical odd frequency ratios along with supplementary movies to illustrate the synchronization behavior (SI-2∼9, ESI†). For the frequency ratio of $R_f = 7/5$, the bead moved "three steps forward and two steps back" (SI-4, Fig. 4[E]); conversely when $R_f = 9/5$, the bead instead moved in a forward-back-forward-forward-back pattern (SI-5, ESI,† Fig. 4[F]). Trajectories for frequency ratios $R_f = 1$ (SI-2, ESI,† Fig. 4[A]), $R_f = 3$ (SI-3, ESI,† Fig. 4 [B]), $R_f = 5/3$ (SI-6, ESI,† Fig. 4[C]) and $R_f = 7/3$ (SI-7, ESI,† Fig. 4[D]) are also provided.

For all even or irrational frequency ratios, the beads displayed only closed orbits even though in some cases the beads moved several hundred magnets before returning to their original position. In one example, shown in Fig. 4[J] ($R_f = 49/50$), the bead moves 20 magnets before returning to its original position (SI-8). In comparison, for $R_f = 2$ the bead is restricted nearby its original lattice position (SI-9, ESI,† Fig. 4[I]). Fig. 5 shows a comparison of experiment and simulation for the oscillation

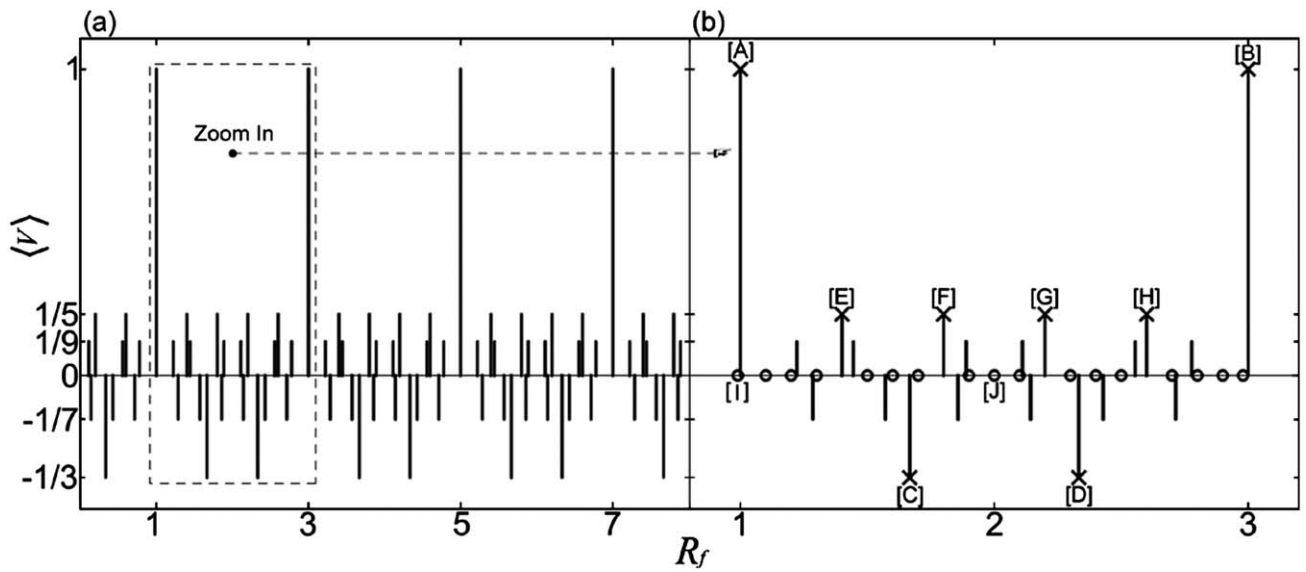

Fig. 3 Velocity Spectra The time-averaged velocity $\langle V\rangle = X/N_{cycle}$ is presented as a function of the frequency ratio, R_f. **(a)** A large view of the velocity spectra is shown and a zoom-in view within the region $1.0 \le R_f \le 3.0$ is provided in **(b)**. The × and ○ markers represent the experimentally observed open and closed trajectories which are depicted in Fig. 4.

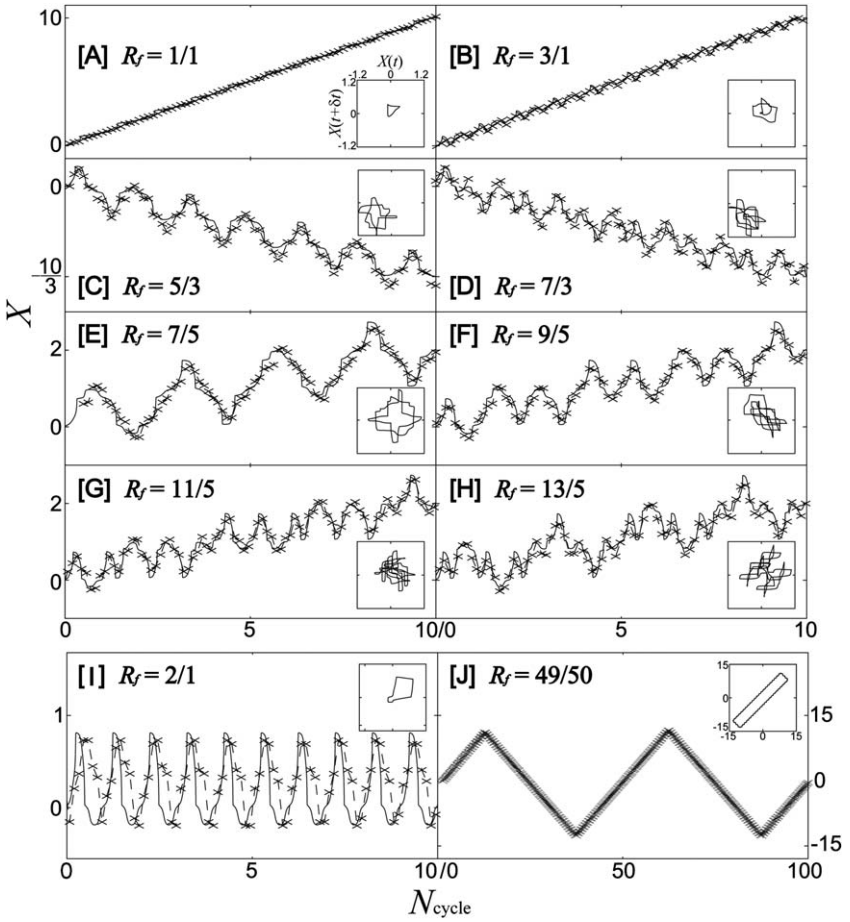

Fig. 4 Open and Closed Trajectories. Comparison of the experimental and numerically simulated trajectories for frequency ratios of [A] 1/1, [B] 3/1, [C] 5/3, [D] 7/3, [E] 7/5, [F] 9/5, [G] 11/5 and [H] 13/5 is provided. The time-averaged velocities of [A∼B] are 1^{-1}, [C∼D] are -3^{-1} and [E∼H] are 5^{-1} respectively. The trajectories of closed orbits are shown for two different frequency ratios of [I] 2/1 and [J] 49/50. The × markers present the experimental results and the solid lines are numerically simulated results. The embedded plots in each panel are the delay mapping $X(t)$ *vs.* $X(t + \delta t)$ to demonstrate the periodicity of the motion with the delay of a quarter of a period.[39]

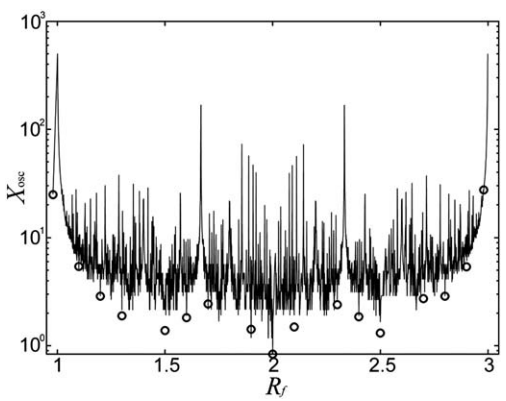

Fig. 5 Oscillation Spectrum. The range of oscillation is provided as a function of frequency ratio in the range $0.98 \leq R_f \leq 3$. The ○ markers are the experimentally verified points. When R_f approaches an odd integer frequency ratio, X_{osc} approaches infinity, which results the spikes in the spectrum.

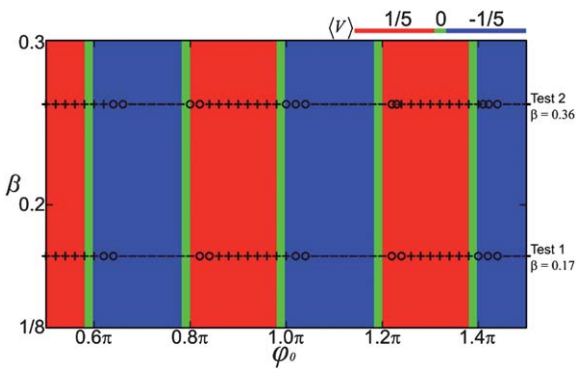

Fig. 6 Phase Effect on Bead Mobility and Multiplexed Separation. The time–averaged velocity as a function of φ_0 and β for fixed frequency ratio of $R_f = 7/5$ is provided. The red, green and blue regions represent positive, zero, and negative velocities, respectively. The experimental results for the velocities of the 2.7μm and 5.8μm beads under different φ_0 are provided as +'s, −'s and ○'s for positive, negative and zero velocity, respectively. The slight offset in the two experimental datasets show that this effect can be used to achieve high resolution particle separation and forms the basis of future separation apparatuses. Supplementary movies are provided in SI-10 and SI-11 which illustrate this concept.

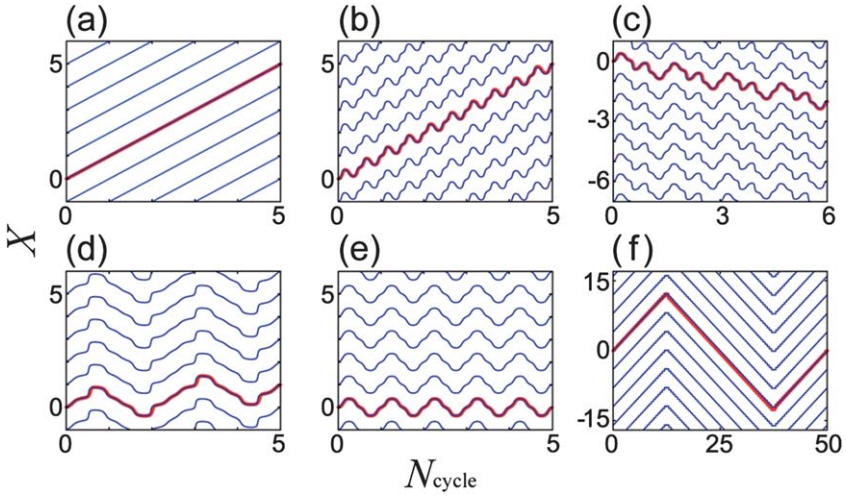

Fig. 7 **Analytical solutions**. The red bold lines are simulated with eqn (5) and the blue lines are simulated with eqn (8) with frequency ratios: (a) 1/1, (b) 3/1, (c) 7/3, (d) 7/5, (e) 2/1 and (f) 49/50.

range in closed trajectories, *i.e.*, $X_{osc} = X_{max} - X_{min}$ as a function of the frequency ratio.

The initial phase difference, φ_0, was found to control not only the direction of the motion, but also whether trajectory is open or closed. In this demonstration, we used large beads with mean diameter of 5.8μm for comparison against the smaller 2.7μm beads used in the majority of this work. For the fixed frequency ratio of $R_f = 7/5$ and $\omega_x = \pi$ rad s^{-1}, we numerically simulated the motion as a function of φ_0 and $\beta = a/d$ in order to map out the β *vs.* φ_0 phase space (Fig. 6). Three distinct regimes of motion having positive (red), zero (green), or negative (blue) time-averaged velocities were observed for the two bead types (*i.e.*, $\beta = 0.17$ and 0.36).

Although the bead motion as a function of φ_0 does not depend strongly on β (small and large beads switch their direction of motion at nearly the same phase), experimentally there was a narrow window where multiplexed magnetic separation could be achieved. For example, at one phase only the small beads had open trajectories (see SI-10, ESI,†, for $\varphi_0 = 150°$) whereas at another phase only the large beads had open trajectories (see SI-11, ESI,†, for $\varphi_0 = 158°$). These results demonstrate the ability to turn ON or OFF the mobility of different bead types using phase modulation control. Due to variability among the beads and substrate, not all the beads displayed exactly the phase dependent velocity; however, these results are a promising indicator that multiplexed separation systems can be devised.

V. Discussion

The condition of open trajectories occurring only for odd integer frequency ratios has been postulated to arise from symmetry arguments of even and odd spatial and temporal functions,[30] however a more rigorous analysis is possible in our case due to our ability to experimentally visualize the particle trajectories. Consider the simplest possible periodically charged substrate with monochromatic, unidirectional periodicity ($n = 1$ and $m = 0$). Assuming $d_M = d/2$, the normalized velocity is:

$$\dot{\xi}_x = \omega_0[\cos(\xi_x)\sin(\omega_x t) - \sin(\xi_x)\sin(\omega_z t + \varphi_0)] \quad (5)$$

where $\omega_0 = 2\pi F_0/6\pi\eta ad \approx 145$ rad s^{-1} is the characteristic frequency of the system, related to the applied force and friction coefficient. Making use of the transformation, $\cos(\xi_x) = \dot{\xi}_x^{-1}(d\sin(\xi_x)/dt)$, eqn (5) can be re-written as:

$$\dot{\xi}_x^2 = \left[-\frac{\omega_0}{\omega_x}\frac{d\sin(\xi_x)}{dt}\frac{d\cos(\omega_x t)}{dt} + \frac{\omega_0}{\omega_z}\frac{d\cos(\xi_x)}{dt}\frac{d\cos(\omega_z t + \varphi_0)}{dt}\right] \geq 0 \quad (6)$$

which reveals that the kinetic energy of the integral is positively bounded, and in the adiabatic limit of either large characteristic forcing or slow driving, ω_x, $\omega_z \ll \omega_0$, will approach the lower bound and permit an asymptotic solution. Temporal periodicity in the multifrequency excitation allows us to perform an endpoint analysis by evaluating the position of a bead after one half of a mutual driving cycle of the two frequencies, *i.e.* $t_f = t_i + (2T_{mut})^{-1}$, where T_{mut} is the lowest common period of the two frequencies. Upon integrating (6) once we have:

$$R_f d\sin(\xi_x)\int_{t_i}^{t_f} d\cos(\omega_x t) = d\cos(\xi_x)\int_{t_i}^{t_f} d\cos(\omega_z t + \varphi) \quad (7)$$

which shows that the time integral will be non-zero only if the ratio, ω_z/ω_x, is composed of odd integers. In other words, the temporal shift between the initial and final states after one half mutual driving cycle, $\omega_{x,z}\cdot T_{mut}/2$ will be an odd integer of π when ω_x or ω_z are both odd, and otherwise will be an even integer of π if either ω_x or ω_z is even. Therefore, for systems containing even integer driving frequencies, the integral of (7) must vanish identically, implying that the initial and final positions after one half of a mutual driving cycle must be the same, $\xi_x(t_i) = \xi_x(t_f)$, *i.e.* a bounded trajectory. Alternatively, if neither side eqn (7) vanishes, then there are no restrictions on the initial and final positions of the bead, and a range of open orbits are possible. In

the adiabatic limit, we can therefore solve the trajectory by setting eqn (5) equal to zero, leading to:

$$\xi_x = \tan^{-1}\left(\frac{\sin(\omega_x t)}{\sin(\omega_z t + \varphi_0)}\right) \quad (8)$$

A comparison plot of the numerical simulation of (eqn (5)) and our analytical result (eqn (8)) is presented in Fig. 7, using $\varphi_0 = \pi/2$ as an example, to show that the range of trajectories are open (closed) for odd (even) integer ratios, respectively. Furthermore, a simple analysis of the phase modulation demonstrates that the trajectories switch in a manner consistent with Fig. 6. What result (8) does not elucidate is the size dependence of the phase control, and it remains an open question as to why different particles can move in opposite directions on the same ratchet potential.[14] Future work can shed light on this fascinating question and open the way for biological sensing and separation applications that need to detect and purify different components within a polydisperse mixture (*e.g.*, cells, bacteria).

VI. Conclusion

Here we have explored the non-linear dynamics of magnetic beads exposed to a multi-frequency magnetic ratchet. Through a combination of theory, simulation, and experiment, we have arrived at several conclusions: (i) open transport is possible only for two driving frequencies that are odd integer ratios, (ii) the initial phase difference between the driving fields can induce flux reversal in the direction of the object's motion, and (iii) there is experimental evidence that colloidal objects of different sizes can be sorted by controlling the initial phase difference between the driving fields. These results open up a new platform for multiplexing the motion of colloidal beads on a miniaturized chip-based platform, which adds flexibility by allowing both the smaller particles to move at the expense of the bigger ones and *vice versa* – something which is not possible with conventional frequency based control mechanisms that employ bifurcation behavior between phase-slipping and phase-locked dynamics. These results enable future improvements in the ability to sort cells, bacteria, pathogens and other colloidal objects in a microchip format, and in addition they provide new theoretical and experimental insights on the fundamentals of ratchet behavior that may find applications in other fields.

Acknowledgements

The authors are thankful for NSF support from grant CMMI 0800173. The authors are also thankful for Dr Daniel J. Lichtenwalner at North Carolina State University for assistance with evaporation of magnetic thin films.

References

1 O. Lara, X. D. Tong, M. Zborowski and J. J. Chalmers, *Exp. Hematol.*, 2004, **32**(10), 891–904.
2 K. E. McCloskey, J. J. Chalmers and M. Zborowski, *Anal. Chem.*, 2003, **75**(24), 6868–6874.
3 L. R. Moore, M. Zborowski, L. Sun and J. J. Chalmers, *J. Biochem. Biophys. Methods*, 1998, **37**, 11.
4 N. Pamme and C. Wilhelm, *Lab Chip*, 2006, **6**(8), 974–980.
5 P. S. Williams, M. Zborowski and J. J. Chalmers, *Anal. Chem.*, 1999, **71**(17), 3799–3807.
6 L. Cui, D. Holmes and H. Morgan, *Electrophoresis*, 2001, **22**(18), 3893–3901.
7 N. G. Green and H. Morgan, *J. Phys. D: Appl. Phys.*, 1997, **30**(11), L41–L44.
8 K. Gunnarsson, P. E. Roy, S. Felton, J. Pihl, P. Svedlindh, S. Berner, H. Lidbaum and S. Oscarsson, *Adv. Mater.*, 2005, **17**(14), 1730–1734.
9 M. A. Tahir, L. Gao, L. N. Virgin and B. B. Yellen, *Phys. Rev. E: Stat., Nonlinear, Soft Matter Phys.*, 2011, **84**(1), 011403.
10 L. Gao, N. Gottron III, L. N. Virgin and B. B. Yellen, *Lab Chip*, 2010, **10**(16), 2108–2114.
11 B. B. Yellen and L. N. Virgin, *Phys. Rev. E: Stat., Nonlinear, Soft Matter Phys.*, 2009, **80**, 011402–011406.
12 B. B. Yellen, R. M. Erb, H. S. Son, R. Hewlin Jr, H. Shang and G. U. Lee, *Lab Chip*, 2007, **7**(12), 1681–1688.
13 B. B. Yellen, O. Hovorka and G. Friedman, *Proc. Natl. Acad. Sci. U. S. A.*, 2005, **102**(25), 8860–8864.
14 P. Tierno, F. Sagues, T. H. Johansen and T. M. Fischer, *Phys. Chem. Chem. Phys.*, 2009, **11**(42), 9615–9625.
15 P. Tierno, S. V. Reddy, J. Yuan, T. H. Johansen and T. M. Fischer, *J. Phys. Chem. B*, 2007, **111**(48), 13479–13482.
16 A. R. Kose, B. Fischer, L. Mao and H. Koser, *Proc. Natl. Acad. Sci. U. S. A.*, 2009, **106**(51), 21478–21483.
17 Y. Roichman, V. Wong and D. G. Grier, *Phys. Rev. E: Stat., Nonlinear, Soft Matter Phys.*, 2007, **75**(1), 4.
18 S.-H. Lee, K. Ladavac, M. Polin and D. G. Grier, *Phys. Rev. Lett.*, 2005, **94**(11), 110601.
19 M. Pelton, K. Ladavac and D. G. Grier, *Phys. Rev. E: Stat., Nonlinear, Soft Matter Phys.*, 2004, **70**(3).
20 K. Ladavac, K. Kasza and D. G. Grier, *Phys. Rev. E: Stat., Nonlinear, Soft Matter Phys.*, 2004, **70**(1).
21 A. Gopinathan and D. G. Grier, *Phys. Rev. Lett.*, 2004, **92**(13).
22 P. T. Korda, M. B. Taylor and D. G. Grier, *Phys. Rev. Lett.*, 2002, **89** (12), 128301.
23 H. Linke, T. E. Humphrey, A. Löfgren, A. O. Sushkov, R. Newbury, R. P. Taylor and P. Omling, *Science*, 1999, **286**(5448), 2314–2317.
24 D. Cole, S. Bending, S. Savel'ev, A. Grigorenko, T. Tamegai and F. Nori, *Nat. Mater.*, 2006, **5**(4), 305–311.
25 S. Ooi, S. Savel'ev, M. B. Gaifullin, T. Mochiku, K. Hirata and F. Nori, *Phys. Rev. Lett.*, 2007, **99**(20), 207003.
26 S. Savel'ev, F. Marchesoni, P. Hänggi and F. Nori, *Phys. Rev. E: Stat., Nonlinear, Soft Matter Phys.*, 2004, **70**(6), 066109.
27 M. V. Costache and S. O. Valenzuela, *Science*, 2010, **330**(6011), 1645–1648.
28 T. Salger, S. Kling, T. Hecking, C. Geckeler, L. Morales-Molina and M. Weitz, *Science*, 2009, **326**(5957), 1241–1243.
29 R. Gommers, M. Brown and F. Renzoni, *Phys. Rev. A: At., Mol., Opt. Phys.*, 2007, **75**(5), 053406.
30 R. Gommers, S. Denisov and F. Renzoni, *Phys. Rev. Lett.*, 2006, **96** (24), 240604.
31 A. Engel, H. W. Muller, P. Reimann and A. Jung, *Phys. Rev. Lett.*, 2003, **91**(6).
32 S. Matthias and F. Muller, *Nature*, 2003, **424**(6944), 53–57.
33 C.-F. Chou, O. Bakajin, S. W. P. Turner, T. A. J. Duke, S. S. Chan, E. C. Cox, H. G. Craighead and R. H. Austin, *Proc. Natl. Acad. Sci. U. S. A.*, 1999, **96**(24), 13762–13765.
34 J. S. Bader, R. W. Hammond, S. A. Henck, M. W. Deem, G. A. McDermott, J. M. Bustillo, J. W. Simpson, G. T. Mulhern and J. M. Rothberg, *Proc. Natl. Acad. Sci. U. S. A.*, 1999, **96**(23), 13165–13169.
35 A. van Oudenaarden and S. G. Boxer, *Science*, 1999, **285**(5430), 1046–1048.
36 M. Switkes, C. M. Marcus, K. Campman and A. C. Gossard, *Science*, 1999, **283**(5409), 1905–1908.
37 W. K. H. Panofsky; M. Phillips, *Classical Electricity and Magnetism*. Addison Wesley: New York, 1955.
38 O. Hellwig, T. Hauet, T. Thomson, E. Dobisz, J. D. Risner-Jamtgaard, D. Yaney, B. D. Terris and E. E. Fullerton, *Appl. Phys. Lett.*, 2009, **95**(23), 232505–3.
39 S. H. Strogatz, *Nonlinear Dynamics and Chaos with Application to Physics, Biology, Chemistry, and Engineering*. Westview Press: 2000.